

REVIEW ARTICLE

- 1937 **Application of acoustic resonators in photoacoustic trace gas analysis and metrology**
András Miklós, Peter Hess, and Zoltán Bozóki
- OPTICS; ATOMS and MOLECULES; SPECTROSCOPY
- 1956 **Portable, tunable, high-luminosity spherical crystal spectrometer with an x-ray charge coupled device, for high-resolution x-ray spectromicroscopy of clusters heated by femtosecond laser pulses**
F. Blasco, C. Stenz, F. Salin, A. Ya. Faenov, A. I. Magunov, T. A. Pikuz, and I. Yu. Skobelev
- 1963 **Multimass ion imaging detection: Application to photodissociation**
Shang-Ting Tsai, Chih-Kai Lin, Yuan T. Lee, and Chi-Kung Ni
- 1970 **Enhanced Raman sensitivity using an actively stabilized external resonator**
David J. Taylor, Manfred Glugla, and Ralf-Dieter Penzhorn
- 1977 **Tunable pulsed vacuum ultraviolet light source for surface science and materials spectroscopy based on high order harmonic generation**
D. Riedel, J. L. Hernandez-Pozos, R. E. Palmer, S. Baggott, K. W. Kolasinski, and J. S. Foord
- 1984 **Elimination of amplitude-phase crosstalk in frequency domain near-infrared spectroscopy**
S. P. Morgan and K. Y. Yong
- 1988 **The spectral linewidth of tunable semiconductor InAsSb/InAsSbP lasers emitting at 3.2–3.6 μm (2800–3100 cm^{-1})**
A. N. Imenkov, N. M. Kolchanova, Yu. P. Yakovlev, P. Kubát, and S. Civiš
- 1993 **A comparison of glass fluorescers used to measure a pulsed ultraviolet image at F/2**
A. V. Deniz and J. A. Stamper
- 1999 **Quantitative measurement system of molecular orientation by coaxial optical Kerr effect spectroscopy**
Keiji Sakai, Yasuhiro Ikeda, and Kenshiro Takagi
- PARTICLE SOURCES, OPTICS and ACCELERATION, DETECTORS
- 2003 **Application and methodological improvements to the floating-wire technique to characterize the magnetic properties of a spectrometer dipole**
H. J. Stein, G. Krol, S. Barsov, and V. Koptev

(Continued)

- 2011 **Triple drift ion beam bunching systems for enhanced bunching efficiency**
P. R. Sarma, V. S. Pandit, and R. K. Bhandari

NUCLEAR PHYSICS, FUSION and PLASMAS

- 2015 **Liquid impedance matching system for ion cyclotron heating**
K. Saito, Y. Torii, R. Kumazawa, T. Mutoh, T. Seki, F. Shimpo, G. Nomura, M. Yokota, T. Watari, G. Cattanei, and Yangping Zhao
- 2023 **Charge-coupled device systems for recording two-dimensional multi-mega-ampere z-pinch data**
B. H. Failor, P. L. Coleman, J. S. Levine, Y. Song, H. Sze, P. D. LePell, C. A. Coverdale, C. Deeney, L. Pressley, and R. Schneider
- 2032 **Time-resolved measurement on ablative acceleration of foil plates driven by pulsed laser beam**
Hongliang He, T. Kobayashi, and T. Sekine
- 2036 **On the theory of an Omegatron with asymmetric three-dimensional electric fields: Ion trajectories and resonance peak shapes**
P. V. Amerl, H. R. Krouse, and H. Fichtner
- 2043 **Unique broad-spectrum neutron sensing instrument**
J. A. Weaver, M. J. Joyce, A. J. Peyton, J. Roskell, and M. J. Armishaw
- 2048 **Absolute calibration of laser-induced fluorescence experiments by optical depth correction**
St. Franke, A. Dinklage, and C. Wilke
- 2052 **Contamination-free sounding rocket Langmuir probe**
W. E. Amatucci, P. W. Schuck, D. N. Walker, P. M. Kintner, S. Powell, B. Holback, and D. Leonhardt

BASIC PHENOMENA

- 2058 **A double coil apparatus for Barkhausen noise measurements**
E. Puppini, M. Zani, D. Vallaro, and A. Venturi

MICROSCOPY and IMAGING

- 2062 **A high-throughput x-ray microtomography system at the Advanced Photon Source**
Yuxin Wang, Francesco De Carlo, Derrick C. Mancini, Ian McNulty, Brian Tieman, John Bresnahan, Ian Foster, Joseph Insley, Peter Lane, Gregor von Laszewski, Carl Kesselman, Mei-Hui Su, and Marcus Thiebaux
- 2069 **Adaptation to low temperatures of a differential interference contrast microscope with subnanometer sensitivity**
X. Müller, T. Kinoshita, and J. Dupont-Roc
- 2073 **Near-field scanning microwave probe based on a dielectric resonator**
M. Abu-Teir, M. Golosovsky, D. Davidov, A. Frenkel, and H. Goldberger
- 2080 **Detailed description of a compact cryogenic magnetic resonance force microscope**
Doran D. Smith, John A. Marohn, and Lee E. Harrell
- 2090 **A scanning superconducting quantum interference device microscope with high spatial resolution for room temperature samples**
Friederike Gruhl, Michael Mück, Marc von Kreutzbruck, and Jörg Dechert

(Continued)

- 2097 **Superconducting niobium tip for scanning tunneling microscope light emission spectroscopy**
Y. Uehara, T. Fujita, M. Iwami, and S. Ushioda
- 2100 **Scanning noninvasive voltage probe operating at 4.2 K**
A. T. Sellwood, C. G. Smith, E. H. Linfield, M. Y. Simmons, and D. A. Ritchie
- 2106 **Permanent magnet objective lenses for multicolumn electron-beam systems**
A. Khursheed, Z. Yan, and N. Karupiah

CONDENSED MATTER; MATERIALS

- 2110 **Nonmetallic gaskets for ultrahigh pressure diamond-cell experiments**
Daniel Solli and Raymond Jeanloz
- 2114 **Tailoring sphere density for high pressure physical property measurements on liquids**
R. A. Secco, R. F. Tucker, S. P. Balog, and M. D. Rutter
- 2117 **X-ray absorption spectroscopy and imaging of heterogeneous hydrothermal mixtures using a diamond microreactor cell**
John L. Fulton, John G. Darab, and Markus M. Hoffmann
- 2123 **New water shock sensor**
Y. Mori, K. Shimada, M. Nakahara, and K. Nagayama
- 2128 **An apparatus for the measurement of internal stress and thermal expansion coefficient of metal oxide films**
Cheng-Chung Lee, Chuen-Lin Tien, Wean-Shyang Sheu, and Cheng-Chung Jaing
- 2134 **Acoustic resonance in tetramethoxysilane matrices: A new tool to characterize the gel formation**
B. Senouci, S. Serfaty, P. Griesmar, and M. Gindre
- 2139 **Data reduction in 3ω method for thin-film thermal conductivity determination**
T. Borca-Tasciuc, A. R. Kumar, and G. Chen
- 2148 **Automated resonant mechanical analyzer**
E. Bonetti, E. G. Campari, L. Pasquini, and L. Savini

CHEMISTRY

- 2153 **Near-infrared acousto-optic tunable filter based instrumentation for the measurement of dynamic spectra of polymers**
Joseph A. Sweat and David L. Wetzel

BIOLOGY and MEDICINE

- 2159 **A design of mammography units using a quasimonochromatic x-ray source**
M. A. Piestrup, Xizeng Wu, V. V. Kaplan, S. R. Uglov, J. T. Cremer, D. W. Rule, and R. B. Fiorito
- 2171 **Design and testing of high sensitivity microreceiver coil apparatus for nuclear magnetic resonance and imaging**
D. A. Seeber, R. L. Cooper, L. Ciobanu, and C. H. Pennington

ELECTRONICS; ELECTROMAGNETIC TECHNOLOGY; MICROWAVES

- 2180 **Thermal deformation measurement of electronic packages using the atomic force microscope scanning moiré technique**
Y. G. Lu, Z. W. Zhong, J. Yu, H. M. Xie, B. K. A. Ngoi, G. B. Chai, and A. Asundi

(Continued)

- 2186 **A miniature capacitive probe array for transient high voltage capillary discharges**
M. Favre, H. Chuaqui, A. M. Leñero, E. Wyndham, and P. Choi

GENERAL INSTRUMENTS

- 2191 **Frequency-domain fluorescence based fiber optic fire alarm system**
T. Sun, Z. Y. Zhang, and K. T. V. Grattan
- 2197 **Precise pulsed time-of-flight laser range finder for industrial distance measurements**
Ari Kilpelä, Riku Pennala, and Juha Kostamovaara
- 2203 **Digital signal processor-based dc superconducting quantum interference device controller**
Inseob Hahn and Mark Weilert
- 2207 **Novel optical sensor for the measurement of surface texture**
Paolo Tomassini, Luigi Rovati, Giovanna Sansoni, and Franco Docchio
- 2214 **A gas gun for plane and shear loading of inert and explosive targets**
N. K. Bourne and G. S. Stevens

NOTES

- 2219 **Adaptive notch filter-based signal processing method and system for vortex flowmeters**
Ke-Jun Xu, An-Min Wang, and Xun-Hong Lv
- 2221 **Ultracompact autocorrelator for femtosecond laser pulses**
Piotr Wasylczyk
- 2224 **Telecentric viewing system for light collection from a z-pinch plasma**
D. J. Den Hartog and R. P. Golingo
- 2226 **NEW PRODUCTS**
- 2231 **CUMULATIVE AUTHOR INDEX**

Digital signal processor-based dc superconducting quantum interference device controller

Inseob Hahn^{a)} and Mark Weilert

Jet Propulsion Laboratory, California Institute of Technology, Pasadena, California 91109-8099

(Received 24 October 2000; accepted for publication 2 January 2001)

We report on the design and evaluation of a convenient digital signal processor-based (DSP) controller for a dc superconducting quantum interference device (SQUID). Program algorithms for the DSP conveniently replace major functions of an analog flux-locked loop: current bias, modulation signal, demodulation, filtering, integration, feedback, and reset. For the controller described here, the entire system was built using commercially available electronics and sensor units with the addition of a simple operational amplifier circuit for the required gain. The noise level of the nonoptimized dc SQUID controller system at 1 Hz was $\sim 50\mu\Phi_0/\sqrt{\text{Hz}}$. Application of the system was demonstrated as a readout system for a low-temperature magnetic susceptibility thermometer that required flux counting. © 2001 American Institute of Physics.

[DOI: 10.1063/1.1350646]

I. INTRODUCTION

The superconducting quantum interference device (SQUID) and its associated controller have been used in many applications requiring measurements of magnetic-flux changes.¹ A signal from a transducer is coupled to a SQUID sensor at low temperature and a room-temperature flux-locked-loop (FLL) circuit generates a feedback to the sensor to compensate the signal, resulting in operation in a constant flux condition. A typical controller is this FLL mode, and its design is implemented by an analog circuit. The fundamental functions of the FLL are modulation of the flux at the SQUID, lock-in detection of the signal generated by the SQUID, integration of the detected signal, filtering, and feedback. Although conceptually these functions can be easily replaced by a digital signal processor (DSP) and its software, implementation of a DSP-based controller has been rare.² One of the main advantages of using a DSP system to control a SQUID is its convenient manipulations of digitized signals without using additional hardware instruments. For instance, the analog integrator and its reset circuit can be easily implemented by a few lines of code. Fast Fourier transformation, or digital filtering of the signal can be performed in real time. Despite the distinct advantages of digital signal processing over an analog circuit in general, its application to a SQUID system is rare due to the fact that the DSP system generally requires extra effort to develop. Our objective here is to demonstrate the ease of developing such a controller, and to display some of its advantages.

In this work, we present a simple DSP-based SQUID controller system utilizing a commercially available analog-to-digital-digital-to-analog (A/D–D/A) data acquisition PC board with a DSP. We demonstrate the easy application of this controller by applying it to magnetic susceptibility thermometry in a low-temperature physics experiment. To in-

crease the range of the temperature measurements the system is configured to count (up/down) large numbers of flux changes as well. Our DSP SQUID controller simply eliminates the need of an extra computer-interfaced counter circuit (or separate counter software). A low-temperature experiment often requires a temperature controller using a proportional gain and integration [proportional–integral (PI)] of an error signal. We have also successfully combined a simple software PI temperature controller together with the DSP SQUID controller. We emphasize that here we wish to demonstrate the application of a readily available DSP-based PC board with little care given to optimize noise levels and other performance measures.

II. DSP AND FLUX-LOCKED LOOP

The dc SQUID sensor has two Josephson junctions in parallel on a superconducting ring. With constant bias current to the ring, as the total magnetic flux applied to the SQUID ring increases, the voltage across the Josephson junction oscillates with a periodicity of a single flux quantum, $\Phi_0 = 2 \times 10^{-15}$ Wb. The FLL for an analog SQUID electronics system maintains the SQUID at constant voltage (flux) on the steepest slope of the $V-\Phi$ curve. To minimize the effects of low-frequency readout noise and of drift associated with current bias, ac modulation (square or sine wave) at a frequency of 200–500 kHz plus dc feedback is normally applied to the SQUID. In an analog FLL circuit there are many important functions: (1) impedance matching (transformers), (2) preamplifier, (3) variable-gain amplifier, (4) oscillator for the modulation, (5) demodulator, (6) integrator and reset, and (7) low-pass filter. Although there are many parameters which can limit the sensitivity, a carefully designed analog controller can achieve a level of overall noise that is dominated by the intrinsic SQUID noise.³ Our goal in this work is to replace functions (4)–(7) listed above using a commercial A/D and D/A data acquisition PC board with a DSP.

^{a)}Electronic mail: hahn@squid.jpl.nasa.gov

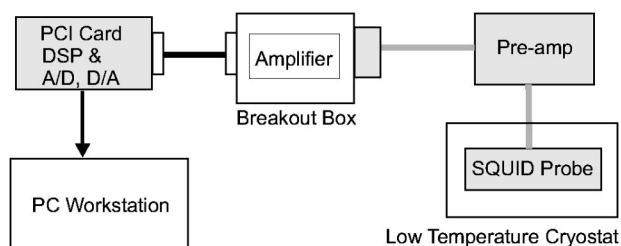


FIG. 1. Block schematic diagram of the DSP-based SQUID controller. The system was built around commercial units (Refs. 4 and 5) indicated as shade except for the break-out box with a home-built amplifier.

In this work, we have used a dc thin-film SQUID sensor and its preamplifier from Quantum Design Inc.⁴ The preamp gain is approximately 400, and the sensor and the input to the preamp are impedance matched using a pair of transformers optimized for the 500 kHz modulation signal of the Quantum Design controller. It is possible to optimize the design for the lower frequency (~ 25 kHz) of the modulation signal employed here, and build the preamp circuit to maximize the signal for this DSP FLL. However, at this time we tried to use readily available instruments and components to reduce the testing time and for more flexibility in experimental arrangements. Figure 1 shows a block schematic of the system.

The DSP board we have used is commercial hardware from Innovative Integration, Inc.⁵ The board was built around the Texas Instruments TMS320C32 digital signal processor capable of up to 30 megainstructions per second (MIPS) (60 MHz clock) performance. The board has a PCI bus interface, memory (512 kWords of program, 256 kWords of data), an input/output (I/O) port and several analog I/O lines. The analog input section features four channels of 16 bit, 100 kHz A/D (Burr-Brown ADS7805). Each channel employs an antialias filter with 50 kHz passband. The board also is equipped with four independent channels of 200 kHz, 16 bit D/A (Analog Devices AD669).

We have built a very simple amplifier in a break-out box to increase the gain of the system using an operation amplifier (Analog Devices AMP01) such that a change of one flux quantum at the SQUID input corresponds to nearly full scale (± 10 V) of the 16 bit A/D. In the break-out box we have current-limiting resistors for feedback and modulation signals. Otherwise, there are no custom-built electronics in this controller system. In this early developmental work we have not emphasized improved shielding and isolation to reduce the computer noise coupled to the SQUID system, for instance, by using optoisolation between analog and digital circuits.

Figure 2 shows more details of the DSP FLL functions. The shaded region represents the program running on the DSP. The maximum frequency of the modulation signal was limited by the speed of the A/D and D/A devices. We have generated a look-up table representing the modulation function (reference signal), and a D/A converts values of the function into an analog signal. This modulation signal is applied directly to the SQUID modulation coil through an electromagnetic interference (EMI) filter and a current-limiting resistor in the break-out box. The resistor value was experi-

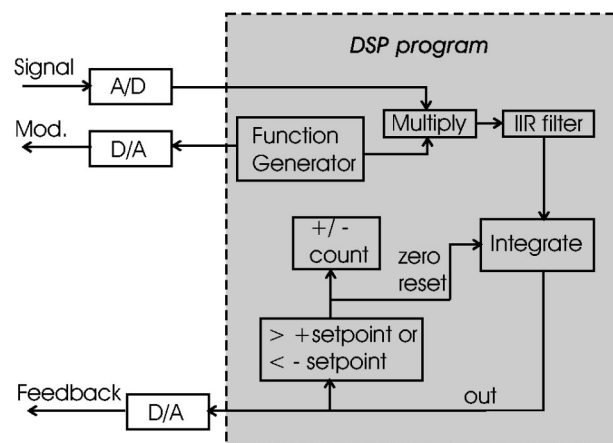


FIG. 2. Schematic diagram of the DSP FLL. The functions inside the dashed box are implemented in DSP programs.

mentally chosen such that the maximum amplitude of the modulation signal (± 10 V) corresponds to a single flux quanta in the SQUID sensor. We have used a sine wave with a frequency of 25 kHz. We expect that a higher modulation frequency will produce an improved signal-to-noise ratio (SNR) because the signal is ac-coupled to the preamp through transformers optimized for higher frequencies.

The next step in the DSP code was to acquire numbers from the A/D representing the amplified SQUID output voltage. To demodulate the continuous-time signal, two numbers (modulation and signal) were synchronously multiplied, then digitally filtered. A simple infinite impulse response (IIR) single-pole, low-pass filter was implemented to suppress harmonics of the modulation frequency in the mixed signal. The filter coefficient was initially chosen such that the cutoff frequency is about 100 samples ($10 \mu\text{s}$ per sample). The integration of the signal was done by a simple accumulation with a scale factor which effectively determines the integrator time constant. The resulting integrated number was then converted to an analog signal (D/A) and fed back to the SQUID sensor through an EMI filter and a feedback resistor in the break-out box. The feedback resistor ($\sim \text{M}\Omega$) was chosen such that a change of flux by a single flux quantum at the SQUID input corresponds to approximately 1/2 full scale of the D/A range. The reset of the integrator to a null value was simply done by two *if* statements. The set point of the reset was chosen to generate a jump of voltage corresponding to one flux quantum after the reset. Counting the reset events to obtain the net flux change is done by simple addition and subtraction of these jumps (± 1) within the reset code. Although it is not shown in Fig. 2, a dc bias current for the SQUID sensor was also digitally generated using a D/A. The dc bias current is adjusted to maximize the SQUID transfer function (see Fig. 3).

The DSP FLL program (schematically shown in Fig. 2) was written using the ANSI-C language and a host computer (Windows-based PC), and was compiled using the Texas Instruments C3x/C4x C compiler. The compiled FLL program was dumped into DSP memory via the PCI bus interface using a PC program provided with the board. Data exchange between the PC processor and the DSP was done using a shared memory buffer on the DSP board accessed

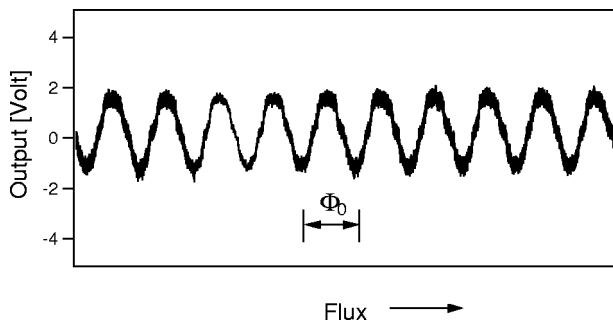


FIG. 3. Demodulator output vs applied flux. Many commercial SQUID electronics also provide this type of detector signal as an output of the unit in a diagnostic mode.

with a simple dynamic-link library (DLL) routine. This DLL function was then called in a program written in LabVIEW (Ref. 6) running on the host computer for the graphical user interface and data storage.

III. TEST RESULTS AND DISCUSSION

Figure 3 shows a typical demodulator signal as a function of flux through the SQUID ring. The demodulator signal is the analog conversion of the IIR filtered numbers (bandwidth ~ 160 Hz) in Fig. 2. A signal varying linearly in time (a ramp) was applied to the input coil of the SQUID sensor for the measurement. The bias current is tuned to maximize the amplitude of the sine wave. The flux-locked loop operates at the steepest slope of the transfer function, $dV/d\Phi \sim \pm 10V/\Phi_0$. The flux noise of the dc SQUID (with shorted input) was measured both using the DSP controller system and a commercial SQUID controller system. The noise of the DSP controller system and that of the commercial system⁷ is, typically, $\sim 50\mu\Phi_0/\sqrt{\text{Hz}}$, and $2\mu\Phi_0/\sqrt{\text{Hz}}$ at 1 Hz, respectively.

The DSP system as implemented here shows higher noise than a commercial analog controller system. However, the commercial preamp circuit and SQUID was designed for the modulation frequency of 500 kHz, while our current modulation frequency was practically limited to 25 kHz (four points using the 100 kHz D/A). Since the SQUID sensor was coupled to the preamp through transformers, we expect that a higher frequency would produce a better SNR. Broadband noise would also be aliased below the Nyquist frequency (50 kHz), resulting in more noise. However, the DSP data acquisition board has a built-in antialias filter which should minimize the aliasing effect. The theoretical maximum slew rate of the DSP FLL can be estimated from the maximum flux error signal and the sample rate. The maximum flux error signal must be less than $\Phi_0/4$, and the maximum slew rate (SR) is given by

$$\text{SR}_{\text{max}} = \frac{\Phi_0 f G}{4},$$

where f is the sampling frequency units of samples per second and G is the gain factor (always less than 1) used in the numerical integration of the error signal. G determines how fast the maximum error signal can be compensated within one sampling cycle, i.e., it is related to the integration time in

the analog integrator circuit. In an ideal noiseless situation the factor G can be 1, meaning the system can integrate the error signal in one sample interval. Thus, the slew rate limit of the system can go up to $25\,000\Phi_0/\text{s}$ using the A/D sampling frequency of 100 kHz in the ideal case. Other factors that limit the slew rate of the system are the D/A output slew rate, the A/D delay, the SQUID and preamp slew rates, and the execution time of the DSP FLL algorithm. We have estimated these factors are negligible compared to the A/D sampling time limit. However, in the real system unavoidable noise should be filtered from the error signal. This filter practically limits the slew rate of our system to roughly $100\text{--}200\Phi_0/\text{s}$. The bandwidth of the system (~ 160 Hz) was effectively determined by the IIR low-pass filter coefficient described in the previous section. The low cutoff frequency was needed to eliminate the noise in the error signal, which caused the DSP FLL frequently to unlock. By improving the EMI suppression, we expect that the bandwidth can be further increased. Although the current system has not been optimized for high-frequency applications, its performance is adequate for many low-frequency applications, for example, for a low-temperature magnetic susceptibility thermometer.

High-resolution thermometers (HRTs) were developed by many groups^{8–12} to study phase transitions in helium at low temperatures. The basic principle of operation is based upon the strong temperature dependence of the magnetization of a paramagnetic salt near its ferromagnetic transition in a magnetic field. The magnetization of the sample is measured by the SQUID magnetometer. The temperature resolution of typical dry (not immersed in liquid helium) HRTs are better than 10^{-9} K near 2 K. The ultimate performance of this type of thermometry is limited by fluctuations in the temperature transducer itself, not by the SQUID readout noise. For instance, the present DSP FLL noise limit of $\sim 50\mu\Phi_0/\sqrt{\text{Hz}}$ would still achieve the typical temperature noise of $10^{-11}\text{K}/\sqrt{\text{Hz}}$ at 1 Hz near 2 K, assuming the temperature transducer sensitivity of $5\Phi_0/\mu\text{K}$. To increase the dynamic range of the temperature measurement, the flux-counting scheme has been traditionally used in HRT systems to track larger flux changes. In the case of the DSP FLL described here, it is trivial to implement the flux counter.

We have used the DSP FLL system in a HRT system. A HRT was installed on a thermal stage with a liquid-helium sample cell (~ 5 cc liquid helium) inside of a low-temperature cryostat. The absolute temperature of the stage was monitored by a calibrated germanium resistance thermometer. The thermometer system will be described in detail elsewhere.¹³ Figure 4 shows the magnetization change of the paramagnetic salt (GdCl_3) as a function of temperature. During the measurement the reset behavior of the system was monitored using an oscilloscope. The FLL became unstable when the single flux quantum reset occurred faster than ~ 120 Hz. This is consistent with the IIR filter cutoff frequency. Although this slew rate limit can be easily increased by using a faster A/D and D/A, typical low-temperature experiments using nano-Kelvin resolution thermometer would

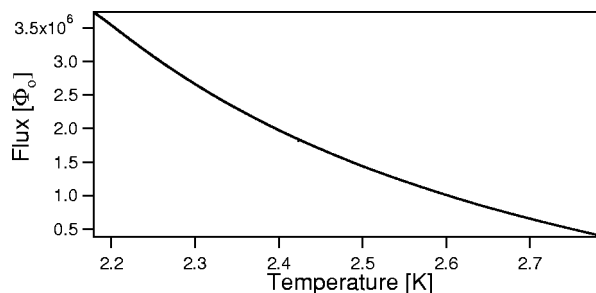


FIG. 4. Magnetization changes of GdCl_3 paramagnetic salt as a function of temperature. The flux counting scheme was used to extend the range of SQUID operation beyond a single flux quanta.

not require a temperature sweep much faster than the limit (~ 0.2 K/h).

We have also implemented a proportional-integral temperature controller within the DSP program. The combined feedback and flux-count numbers were used as the input signal to the PI algorithm. The output of the PI calculation was then converted to an analog signal using a second D/A on the board. The analog signal was used to drive a heater at the thermal stage. The thermal stage was successfully controlled to better than nano-Kelvin stability near 2.1 K using the software PI controller.

In summary, we have developed a DSP-based dc SQUID controller using a commercial data acquisition PC board with a built-in DSP. The performance of the DSP FLL can be improved by using faster A/D and D/A, and by implementing more careful EMI shielding and isolation. Without any effort to develop an optimal instrument, the integrated system using commercial units was successfully used for low-temperature magnetic susceptibility thermometry. Adding more functions (e.g., a temperature controller) to the system

was demonstrated to be extremely easy and flexible. It is also possible to operate many SQUID channels using a single DSP and multiplexed A/Ds and D/As.

ACKNOWLEDGMENTS

The authors have benefited from Paul Welander's experimental support, and from useful discussion with Dr. P. Day. The authors are also indebted to Dr. M. Barmatz and Dr. D. Strayer for careful reading of this manuscript. The research described in this letter was carried out at the Jet Propulsion Laboratory, California Institute of Technology, under contract with the National Aeronautics and Space Administration.

- ¹J. Clarke, in *The New Superconducting Electronics*, edited by H. Weinstock and R. W. Ralston (Kluwer Academic, Dordrecht, the Netherlands, 1993), p. 123. J. Clarke, *Sci. Am.* **271**, 46 (1994).
- ²P. J. Kung, R. R. Bracht, E. R. Flynn, and P. S. Lewis, *Rev. Sci. Instrum.* **67**, 222 (1996).
- ³Commercially available dc SQUID magnetometer systems show, typically, $1 \sim 3 \mu\Phi_0 / \sqrt{\text{Hz}}$ at 100 Hz.
- ⁴Model 50 (dc SQUID sensor), and model 55 (4 m MicroPreamplifier cable): Quantum Design, Inc., San Diego, CA. <http://www.quandsn.com>
- ⁵Model PCI32, Innovative integration, Inc., Westlake Village, CA 91362. <http://www.innovative-dsp.com>
- ⁶LabVIEW is a software from National Instruments, Inc. <http://www.natinst.com>
- ⁷Model 550 (dc SQUID controller), Quantum Design, Inc., San Diego, CA.
- ⁸P. Welander, M. Barmatz, and I. Hahn, *IEEE Trans. Instrum. Meas.* **49**, 253 (2000).
- ⁹P. Day, I. Hahn, T. Chui, A. W. Harter, D. Rowe, and J. Lipa, *J. Low Temp. Phys.* **107**, 309 (1997).
- ¹⁰H. Fu, H. Baddar, K. Kuehn, M. Larson, N. Mulders, A. Schegolev, and G. Ahlers, *J. Low Temp. Phys.* **111**, 49 (1998).
- ¹¹B. J. Klemme, M. J. Adriaans, P. K. Day, D. Sergatskov, T. L. Aselage, and R. V. Duncan, *J. Low Temp. Phys.* **116**, 133 (1999).
- ¹²T. C. P. Chui, D. Swanson, M. J. Adriaans, J. A. Nissen, and J. Lipa, *Phys. Rev. Lett.* **23**, 3005 (1992).
- ¹³P. Welander and I. Hahn (unpublished).